European Conference on Computational Fluid Dynamics
ECCOMAS CFD 2006
P. Wesseling, E. Oñate and J. Périaux (Eds)

AN IMMERSED BOUNDARY METHOD FOR FLOWS AROUND RECTANGULAR OBJECTS.

W.-P. Breugem[*,†]

[*]KNMI, Oceanographic Research Dep.
P.O. Box 201, 3730 AE De Bilt, The Netherlands
e-mail: breugem@knmi.nl
[†]Delft University of Technology, Laboratory for Aero and Hydrodynamics
Leeghwaterstraat 21, 2628 CA Delft, The Netherlands

Key words: Immersed Boundary Method, pressure–correction method, von Neumann stability analysis, porous medium

Abstract. *A second–order accurate and highly efficient Immersed Boundary Method (IBM) is presented for simulating flows along rectangular non–moving solid objects. In this method a rectangular object is placed on a staggered Cartesian grid such that its boundary coincides with grid points for the boundary–normal velocity component. By imposing forces at the grid points nearest to and on the boundary, the no–slip condition for the boundary–parallel velocity components is satisfied exactly, while the no–penetration condition for the boundary–normal velocity component is satisfied to a very good approximation. The accuracy of the IBM requires a pressure–correction method in which the correction pressure is small, which is accomplished by adding a fraction of the correction pressure to the pressure after every time step. It is shown that for the currently used second–order Adams–Bashforth scheme this fraction must not exceed one for maintaining stability. Furthermore, a von Neumann stability analysis has been performed, from which it is argued that the forces imposed in the IBM will usually not affect the numerical stability. The method has been successfully applied to both laminar and turbulent flows through a porous medium consisting of a periodic three–dimensional regular array of cubes.*

1 INTRODUCTION

The Immersed Boundary Method (IBM) is a powerful method for simulating flows in complex geometries. In this method complex geometries are embedded on a computational grid, which usually does not conform to the shape of the geometries. No boundary conditions are specified, but instead in the vicinity of solid boundaries forces are imposed on the flow to enforce the no–slip and no–penetration conditions. As compared to methods using a body–fitted grid, advantages are that the numerical implementation of complex flow geometries is relatively simple, especially in case of moving objects, and that for

Cartesian grids accurate and fast solvers can be used. Throughout the years numerous variants of the IBM have been developed and successfully applied to many different flow problems. A recent overview of the IBM is given by Mittal and Iaccarino[1].

In this paper a new variant of the IBM is presented for rectangular non–moving geometries, which can be aligned along a Cartesian grid. This new variant has an increased accuracy compared to other IBMs in literature that have been applied to rectangular geometries. For example, Leonardi et al.[2] used the IBM of Fadlun et al.[3] for simulating turbulent channel flow over transverse square bars. The method of Fadlun et al.[3] prescribes the prediction velocity at grid points nearest to a solid boundary as calculated from the assumption of a linear profile in the prediction velocity up to the second grid point away from the boundary. The new IBM variant prescribes the prediction velocity only at grid points coinciding with a boundary, where it is put to zero, and does not invoke any assumption on the velocity profile. It has been successfully used in previous studies[4,5] to simulate flow over and through a three–dimensional regular array of cubes.

The structure of this paper is as follows. The IBM is explained in detail in section 2, where also the numerical scheme is given. In section 3 stability restrictions are derived for the pressure update in the pressure–correction scheme. The implications of the IBM for numerical stability are discussed in section 4. The present variant of the IBM has been applied to flow through a periodic three–dimensional regular array of cubes. Numerical results are shown in section 5 for both laminar and turbulent flows. Finally, the main conclusions are summarized and a discussion is given in section 6.

2 NUMERICAL SCHEME AND IMMERSED BOUNDARY METHOD

The finite–volume method is used to discretize the Navier–Stokes equations on a fully staggered and uniform Cartesian grid. Spatial derivatives are discretised according to the central–differencing scheme. The equations are advanced in time with the second–order Adams–Bashforth scheme. The pressure–correction scheme looks as follows:

$$\frac{\tilde{u}_i - u_i^n}{\Delta t} = \frac{3}{2}g_i^n - \frac{1}{2}g_i^{n-1} - \frac{1}{\rho}\frac{dP}{dx}\delta_{i1}, \tag{1}$$

$$\frac{1}{\rho}\frac{\partial^2 \tilde{p}}{\partial x_i^2} = \frac{1}{\Delta t}\frac{\partial \tilde{u}_i}{\partial x_i}, \tag{2}$$

$$u_i^{n+1} = \tilde{u}_i - \frac{\Delta t}{\rho}\frac{\partial \tilde{p}}{\partial x_i}, \tag{3}$$

$$p^{n+1} = p^n + \frac{1}{2}\tilde{p}, \tag{4}$$

where dP/dx is the constant pressure gradient that drives the flow, δ_{i1} is the Kronecker delta, $\tilde{u}_i$ is the prediction velocity, and $\tilde{p}$ is the correction pressure. The function g_i in equation (1) is given by:

$$g_i = -\frac{1}{\rho}\frac{\partial p}{\partial x_i} - \frac{\partial u_i u_j}{\partial x_j} + \nu\frac{\partial^2 u_i}{\partial x_j^2} + f_i, \tag{5}$$

where ν is the kinematic fluid viscosity. Because $\tilde{p}$ plus a constant is a solution as well of equation (2), at every time step the correction pressure is uniformly shifted by a constant such that at a particular fixed point in space it is always zero.

In equation (5), f_i represents the force per unit mass that in the IBM is applied to the flow field to enforce the no-slip and no-penetration conditions on solid boundaries. This is illustrated in figure 1.

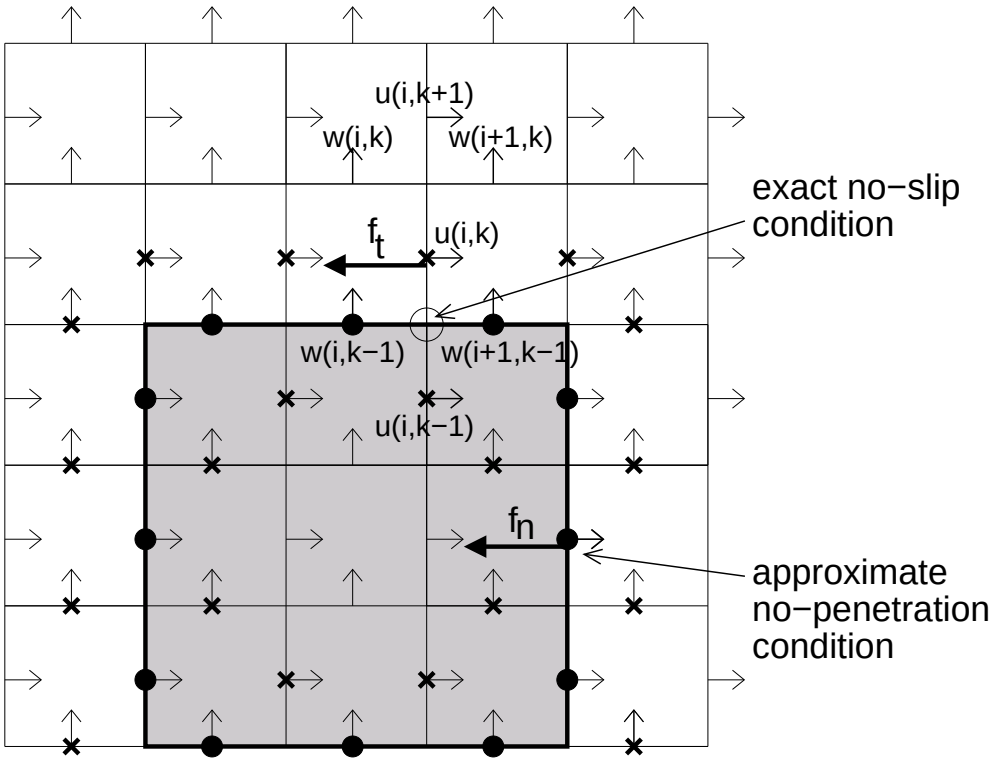

Figure 1: Illustration of the IBM applied to flow along a solid square. The horizontal and vertical vectors mark the grid points for the horizontal and vertical velocity components respectively. The crosses show the grid points at half a grid spacing away from the boundary of the square at which a force f_t is imposed to enforce the no-slip condition on the boundary. The dots show the grid points on the boundary at which the prediction velocity is put to zero, which is equivalent to imposing a force f_n.

The IBM used in this study, applies to a rectangular solid body that can be aligned along grid lines. It consists of three ingredients:

1. The solid body is positioned on the staggered grid such that its boundary coincides with grid points for the velocity component that is directed perpendicular to the boundary. Consequently, the grid points at a distance of half a grid spacing away from the boundary correspond to the other two velocity components that are directed parallel to the boundary.

2. At the grid points at a distance of half a grid spacing away from the boundary, an additional force is imposed in the momentum equation (1) such that the flow experiences an exact no–slip condition for the boundary–parallel velocity components at the boundary:

$$\mathbf{u} \times \mathbf{n} = \mathbf{0}, \tag{6}$$

where $\mathbf{n}$ is the normal vector on the boundary. As an example we derive an expression for the force f_t at position (i,k) in figure 1 that is equivalent to imposing a zero boundary–parallel velocity at the location of the circle on the boundary of the square. The discretised terms in equation (5) that contain the velocity components $u_{(i,k-1)}$, $w_{(i,k-1)}$ and $w_{(i+1,k-1)}$, are:

$$\begin{aligned} -\left.\frac{\partial uw}{\partial z}\right|_{(i,k)} &= -\left[\frac{uw|_{(i,k+1/2)} - uw|_{(i,k-1/2)}}{\Delta z}\right], \\ \nu\left.\frac{\partial^2 u}{\partial z^2}\right|_{(i,k)} &= \nu\left[\frac{u_{(i,k+1)} - 2u_{(i,k)} + u_{(i,k-1)}}{\Delta z^2}\right], \end{aligned}$$

where $uw|_{(i,k-1/2)}$ corresponds to uw at the location of the circle. According to the desired no–slip condition, $uw|_{(i,k-1/2)} = 0$ and $u_{(i,k-1)} = -u_{(i,k)}$ must hold. This is equivalent to a force f_t equal to:

$$f_t|_{(i,k)} = -\frac{uw|_{(i,k-1/2)}}{\Delta z} - \nu\left[\frac{u_{(i,k)} + u_{(i,k-1)}}{\Delta z^2}\right]. \tag{7}$$

3. At the grid points on the boundary the prediction velocity is put to zero. According to equation (3) this yields a small penetration (or boundary–normal) velocity equal to:

$$\mathbf{u}^{n+1} \cdot \mathbf{n} = -\frac{\Delta t}{\rho}\nabla\tilde{p} \cdot \mathbf{n} \approx 0. \tag{8}$$

To keep the penetration velocity small, it is essential that the gradient of the correction pressure correction remains small. This is accomplished by updating the pressure after every time step by adding to it a fraction of the correction pressure, see equation (4). Because Δt is also small, the right–hand side of (8) will therefore be very small compared to velocities in the surrounding of the body. For stationary flows the correction pressure is expected to approach zero, in which case the no–penetration condition is enforced exactly.

A formal accuracy test of the IBM has not been performed. It is however likely that it is second–order accurate, as it should at least be as accurate as the second–order accurate IBM of Fadlun et al.[3]. Fadlun et al.[3] assume a linear profile in the prediction velocity up

to the second grid point away from the boundary, while in the present method nothing is assumed on the velocity profile. It is noted that the method of Fadlun et al.[3] has been developed with a different aim compared to the present method, and is still considered as valuable for complex flow geometries not aligned along a grid.

The interior of a solid object may be treated in different ways without affecting the flow outside the solid object. In the simulations shown in this paper, forcing is applied not only at grid points outside, but also inside an object. Consequently, the IBM forces are smeared out over about twice as many grid points and are therefore roughly twice as small as compared to the case with forcing applied only outside objects. Another consequence of this is that the interior of a solid object is similar to a closed cavity in which the 'flow' is at rest. In the simulations also the pressure forcing (dP/dx) in equation (1) is put to zero inside a solid object. This implies that inside objects the pressure p is a constant. If the pressure forcing would not be turned off inside objects, a streamwise linear pressure profile develops to balance the forcing:

$$p(x) = \frac{dP}{dx}x + \text{constant}.$$

3 RESTRICTIONS FOR THE PRESSURE UPDATE

The IBM proposed in this paper requires a small correction pressure in order to keep the penetration velocity, as given by equation (8), sufficiently small. For this reason the pressure is updated every time step according to equation (4). In this section it is shown that for the pressure to remain bounded, the fraction of the correction pressure added to the pressure must be in between zero and one. In the analysis below equation (4) is replaced by

$$p^{n+1} \;=\; p^n + \gamma\,\tilde{p}^n, \tag{9}$$

with γ a real number and $\tilde{p}^n$ the correction pressure at time step n.

Let us substitute equation (3) into equation (1) and rewrite the result according to:

$$\begin{aligned}\frac{\left(u_i^{n+1}-u_i^n\right)}{\Delta t} \;=\; & -\frac{1}{\rho}\frac{\partial\left[\frac{3}{2}p^n-\frac{1}{2}p^{n-1}+\tilde{p}^n\right]}{\partial x_i}-\frac{1}{\rho}\frac{dP}{dx}\delta_{i1}\\ & +\frac{3}{2}\left(g_i+\frac{1}{\rho}\frac{\partial p}{\partial x_i}\right)^n-\frac{1}{2}\left(g_i+\frac{1}{\rho}\frac{\partial p}{\partial x_i}\right)^{n-1}.\end{aligned} \tag{10}$$

For stationary or quasi–stationary flows with $|u_i^{n+1}-u_i^n| \ll \Delta t$, the right-hand side of this equation must also be stationary or quasi–stationary. This holds automatically for the last three terms on the right–hand side, because the second term is a constant and the third and the fourth term are evidently stationary when the velocity is stationary. This is, however, not trivial for the first term on the right–hand side. For stationary flows it is therefore explicitly required that:

$$\frac{3}{2}p^{n+1} - \frac{1}{2}p^n + \tilde{p}^{n+1} = \frac{3}{2}p^n - \frac{1}{2}p^{n-1} + \tilde{p}^n. \tag{11}$$

By combining equations (9) and (11) the following recurrence relation is obtained for the correction pressure:

$$\tilde{p}^{n+1} = \left(1 - \frac{3}{2}\,\gamma\right)\tilde{p}^n + \frac{1}{2}\gamma\,\tilde{p}^{n-1}. \tag{12}$$

For convergence it is required that $|\tilde{p}^{n+1}/\tilde{p}^n| \leq 1$. The boundary of the domain of γ for which convergence exists is found from putting $\tilde{p}^{n+1} = e^{I\phi}\tilde{p}^n$, with $\phi \in [0, 2\pi)$ and I the imaginary unit, into equation (12):

$$\gamma = \frac{3 - 4e^{I\phi} + e^{I2\phi}}{5 - 3\cos\phi}. \tag{13}$$

The result is shown in figure 2. Noting that γ is a real number, it follows that the

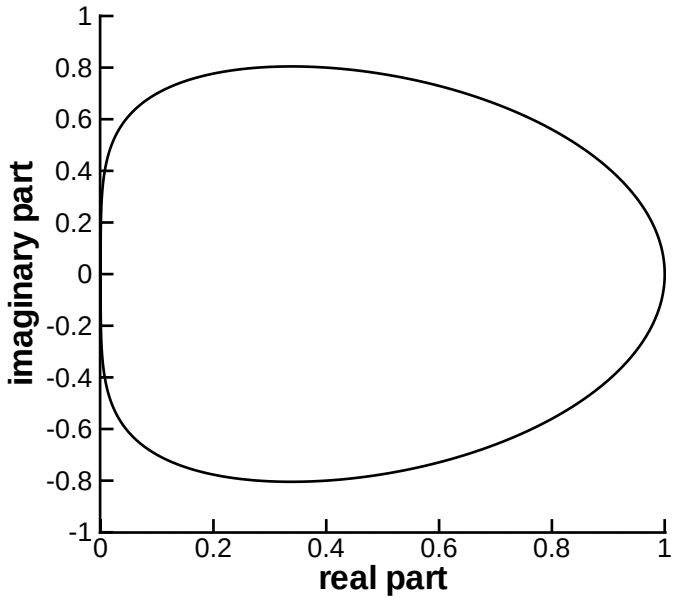

Figure 2: Convergence domain for γ as given by equation (13).

correction pressure remains bounded for $0 \leq \gamma \leq 1$. Of course $\gamma = 0$ is not recommended for the accuracy of the IBM. Furthermore, from simulations of stationary flow through an array of cubes, as discussed in section 5, it is found that for $\gamma = 1$ the correction pressure does not converge to zero, but to a steady oscillation with $\tilde{p}^{n+1}/\tilde{p}^n = -1$ conform to

equation (12). Therefore, although the use of $\gamma = 1$ is widespread, for the simulations shown in this paper $\gamma = 0.5$ has been taken. Test simulations revealed no change in the velocity field for these two different values of γ.

The analysis above has been based on the assumption of stationary flow. For instationary flows, however, the same restrictions for γ are expected, as usually in parts of the flow domain, e.g. near walls, the flow may be close to a quasi–stationary state.

The value of γ may affect the temporal accuracy of the velocity and more in particular the pressure. For the case of $\gamma = 0$, Wesseling[6] (p. 254) mentions that the global temporal accuracy of the velocity is $O(\Delta t^2)$, while he expects at least $O(\Delta t)$ for the pressure (which for $\gamma = 0$ is given by the correction pressure). For the case of $0 < \gamma \leq 1$ the same accuracy for the velocity is expected, but increased accuracy for the pressure, although this has not been formally tested.

4 IMPLICATIONS IBM FOR NUMERICAL STABILITY

The IBM forces may affect the stability of the numerical scheme. In previous studies[4,5] it was suggested that the IBM forces may cause large negative shifts in the real part of the eigenvalues of g_i given by equation (5). This motivated the choice for a time integration scheme that allowed for eigenvalues with a larger negative real part as compared to the Adams–Bashforth scheme currently used. However, based on a similar von Neumann stability analysis as given in Wesseling[6] (sections 5.6–5.8), it will be shown that in fact the IBM forces do not affect the extremes of the real, but only of the imaginary part of the eigenvalues. Furthermore, it will be argued that it is likely that the IBM forces do not affect the stability at all.

In the von Neumann stability analysis we neglect the first term on the right–hand side of equation (7) for the IBM force f_t, because according to equation (8) the boundary–normal velocity on the solid boundary is very small:

$$f_t \approx -\nu \left[\frac{u_{(i,k)} + u_{(i,k-1)}}{\Delta z^2} \right].$$

We consider the same instationary convection–diffusion equation as in Wesseling[6] (p. 175), except for an additional force term f_t:

$$\frac{\partial u}{\partial t} + Lu = 0, \quad Lu = \sum_{l=1}^{3} \left(U_l \frac{\partial}{\partial x_l} - \nu \frac{\partial^2}{\partial x_l^2} \right) u - f_t, \tag{14}$$

where the velocities U_l are assumed to be constant. The above equation is discretised with the central–differencing scheme on a uniform grid. The discretization L_Δ of the operator L becomes:

$$\begin{aligned} \Delta t L_\Delta u_m \;=\; & \frac{1}{2} \sum_{l=1}^{3} c_l \left(u_{m+e_l} - u_{m-e_l} \right) + \\ & \frac{1}{2} \sum_{l=1}^{3} d_l \left(-u_{m+e_l} + 2u_m - u_{m-e_l} + \alpha_l \left[u_m + u_{m-e_l} \right] + \beta_l \left[u_m + u_{m+e_l} \right] \right), \end{aligned} \tag{15}$$

where $m = (i, j, k)$ the index of the grid point, $e_1 = (1, 0, 0)$, $e_2 = (0, 1, 0)$, $e_3 = (0, 0, 1)$, $c_l = U_l \Delta t / \Delta x_l$ the CFL number, $d_l = 2\nu \Delta t / \Delta x_l^2$ the diffusion number, and α_l and β_l indicator functions for the IBM forces. If at a grid point no IBM force is imposed, then $\alpha_l = \beta_l = 0$ for $l = 1..3$, and else $\alpha_l = 1$ and/or $\beta_l = 1$ for certain l. For example, at point (i, k) in figure 1, $\alpha_3 = 1$ and $\alpha_1 = \beta_1 = \beta_3 = 0$, while at point $(i, k-1)$, $\beta_3 = 1$ and $\beta_1 = \alpha_1 = \alpha_3 = 0$.

Following Wesseling[6] we define the discrete Fourier Transform $\mathcal{F}\{L_\Delta\}$ of L_Δ by:

$$\mathcal{F}\{L_\Delta\} \;=\; e^{-Im\theta} L_\Delta e^{Im\theta},$$

with $m\theta = \sum_{l=1}^{3} m_l \theta_l$, $\theta_l = 2\pi k_l / N_l$ the wavenumber in the l^{th} direction with N_l the (even) number of grid points in this direction and $k_l = -N_l/2 + 1, .., N_l/2$ an integer number. The expression for $\mathcal{F}\{L_\Delta\}$, which is in fact the eigenvalue of L_Δ, reads:

$$\Delta t \, \mathcal{F}\{L_\Delta\} = 2 \sum_l d_l s_l + I \sum_l \hat{c}_l \sin\theta_l, \tag{16}$$

with $s_l = (1 - \alpha_l/2 - \beta_l/2) \sin^2(\theta_l/2) + (\alpha_l + \beta_l)/2$ and $\hat{c}_l = c_l + d_l \left(\beta_l - \alpha_l\right)/2$ the modified CFL number. The Fourier Transform has the same form as in Wesseling[6] (p. 176), with only a modified CFL number and a modified expression for s_l. Without loss of generality we may assume that $\hat{c}_l \geq 0$. We note furthermore that $0 \leq s_l \leq 1$ always holds, irrespective the values of α_l and β_l. From this it follows that the IBM forces do not affect the extremes of the real part of the eigenvalues of $\Delta t L_\Delta$.

For numerical stability it is required that $\Delta t \, \mathcal{F}\{L_\Delta\}$ is inside the stability domain of the second–order Adams–Bashforth scheme. From this the constraints for the time step Δt can be derived. The analysis is identical to that given in Wesseling[6] as the form of equation (16) is the same as in his analysis. The constraints for the time step become[3] (p. 188):

$$\frac{\nu \Delta t}{\Delta x^2} \;<\; \frac{1}{12}, \tag{17}$$

$$\frac{\Delta t \sqrt{\sum_l \left[U_l + \frac{\nu}{\Delta x}(\beta_l - \alpha_l)\right]^2}}{\Delta x} \;<\; \frac{1}{3}, \tag{18}$$

$$\sum_l \left(\frac{\Delta t |U_l + \frac{\nu}{\Delta x}(\beta_l - \alpha_l)|}{\Delta x} \right) \left(\frac{|U_l + \frac{\nu}{\Delta x}\left(\beta_l - \alpha_l\right)| \Delta x}{\nu} \right)^{1/3} \;<\; 2^{1/3}, \tag{19}$$

where it is used that in our simulations $\Delta x = \Delta y = \Delta z$.

Provided that the grid resolution is sufficiently high, at the grid points where the IBM force f_t is imposed, the flow is in the viscous regime with the local Reynolds number $|U_l| \Delta x / \nu \leq O(1)$. It is not difficult to show that for $|U_l| \Delta x / \nu < 1$ condition (17) is most restrictive. Based on this it may be expected that there will be usually little or no effect of the IBM forces on numerical stability.

5 NUMERICAL RESULTS

The flow geometry considered in the present work is a fully periodic three–dimensional regular array of cubes shown in figure 3. It is a model geometry of a simple porous medium with an isotropic permeability. In the simulations the cube rib was taken equal to the distance in between the cubes, i.e. $d_f = d_p$, which corresponds to a porosity or void fraction of 0.875. The flow is driven by a net horizontal pressure gradient in the x–direction.

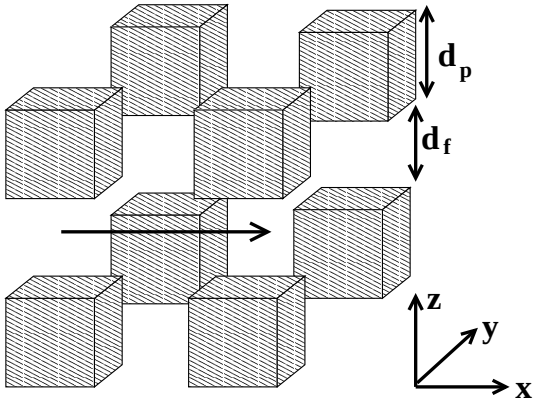

Figure 3: Sketch of the flow geometry: a fully periodic three–dimensional regular array of cubes.

The IBM of section 2 was applied to enforce a zero velocity on the cubes. Because of the continuous computational domain with periodic boundary conditions, a fast, accurate and FFT–based direct solver could be used for the pressure Poisson equation (2). The maximum time step allowed for numerical stability was estimated from equations (17)–(19).

Results are presented from two simulations with a different Reynolds number, $Re_p = \langle u \rangle^s d_p/\nu$, where $\langle u \rangle^s$ is the so–called superficial volume–averaged velocity. The latter is defined here according to:

$$\langle u \rangle^s = \frac{1}{V} \int_{V_f} u \, dV,$$

with $V = (d_f + d_p)^3$ the volume of a unit cell of the array of cubes and $V_f = V - d_p^3$ the volume of the (true) fluid inside this unit cell.

In the first simulation the Reynolds number is very low, $Re_p = 0.0122$, at which the flow is in the viscous regime and stationary. Figure 4 shows a cross–section of the flow field along with contours of the pressure. The flow is resolved on 40x40x40 grid points and a fully periodic domain with dimensions $2d_p \, \mathrm{x} \, 2d_p \, \mathrm{x} \, 2d_p$ in respectively the x, y and z–direction. The maximum allowed time step was found to be limited by condition (17), and thus was not affected by the IBM. The time step was put equal to half the maximum allowed value at $\Delta t \nu/(\Delta x)^2 = 1/24$. Figure 4 exhibits mirror symmetry at $z/d_p = 1$ in

the velocity and pressure field, as expected, which indicates that the IBM forces have been implemented correctly in the numerical code. Furthermore, velocities and pressures inside the cube appear to be zero at machine precision, confirming that for stationary flows the IBM captures the exact no–slip and no–penetration conditions.

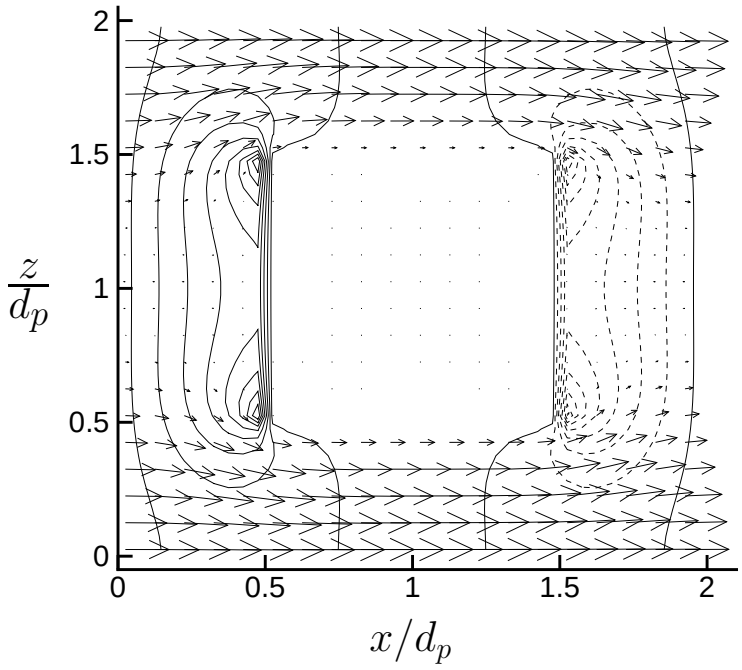

Figure 4: Cross–section of the flow field at $Re_p = 0.0122$ with cut through the middle of the cube. Vectors represent the velocity field, with 1 out of every 2 vectors shown. Contours denote the pressure field, solid for positive and dashed for negative pressures relative to a zero reference pressure at the center of the cube.

In the second simulation the Reynolds number is much higher, $Re_p \approx 430$, at which the flow is in the turbulent regime. A snapshot of the flow field is shown in figure 5. The flow has been resolved on 192x96x96 grid points and a fully periodic domain with dimensions $4d_p \,\mathrm{x}\, 2d_p \,\mathrm{x}\, 2d_p$ in respectively the x, y and z–direction. The maximum allowed time step was set by condition (18) in regions with high velocity, away from the cube boundaries. Thus, like for the stationary case, also in this case the IBM did not affect the numerical stability. The time step was fixed in time at a value of $\Delta t\langle u\rangle^s/\Delta x = 0.066$, more than twice as small as the typical maximum allowed time step. Figure 5.b shows the velocity field inside the cubes after being magnified by a factor of 10^4. The highest velocities inside the cubes are found to be $O(10^4)$ times smaller than $\langle u\rangle^s$. To be more precise: at the instant of time corresponding to figure 5, the highest penetration velocity was located on the lower front side of the left cube with a value equal to $1.2 \cdot 10^{-4}\langle u\rangle^s$. The contours

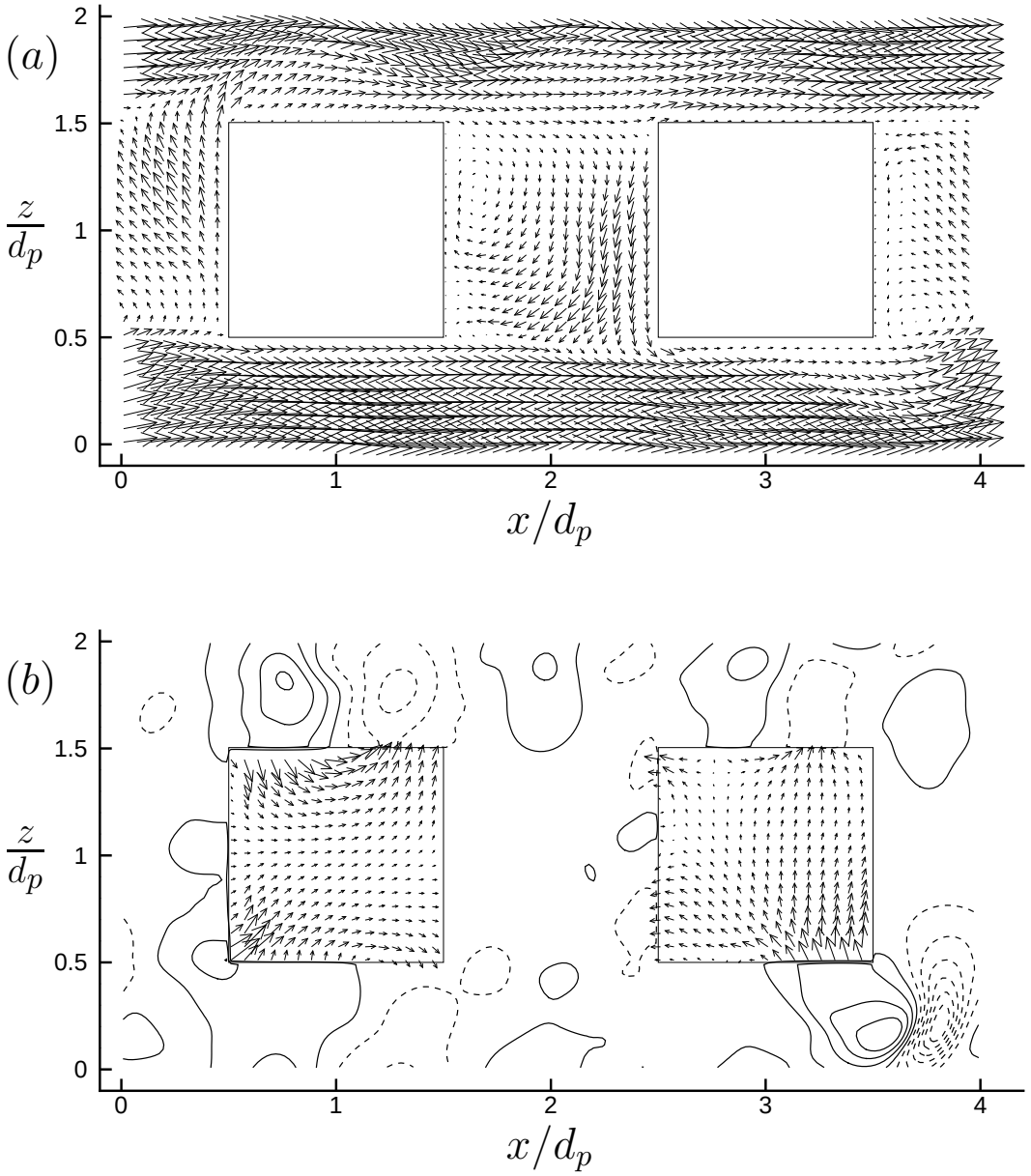

Figure 5: Two–dimensional snapshot of the flow field at $Re_p \approx 430$ with cut through the middle of the cubes. (a) Velocity field, with 1 out of every 3 vectors shown. (b) Velocity field inside the cubes, multiplied by 10^4, along with the corresponding pressure correction field. Solid (dashed) contours for positive (negative) pressures relative to a zero reference pressure in the center of the left cube. The length of the reference vector for (a) and (b) is the same.

in figure 5.b represent the pressure correction field. The velocities inside the cubes are

clearly driven by the distribution of the pressure correction field at the boundaries of the cubes, as expected from equation (8).

6 CONCLUSIONS AND DISCUSSION

The numerical results demonstrate the high accuracy of the IBM for rectangular flow geometries. For stationary flows the no–slip and no–penetration conditions are enforced at machine precision, while in the example of a turbulent flow negligible small penetration velocities existed on the cube boundaries of $O(10^4)$ times smaller than the superficial volume–averaged velocity. Unlike methods that assume a linear profile in the prediction velocity up to the second grid point away from a boundary, the present method does not assume anything on the velocity profile near boundaries.

The IBM has second–order accuracy and appears not to influence the numerical stability in the examples shown. As argued in section 4, the effect of the IBM on numerical stability can usually be neglected. The method demands little computational overhead for calculating forces and solving the flow inside solid objects, but has the major advantage that it enables the use of efficient solvers for the pressure Poisson equation.

The IBM requires a pressure–correction scheme in which the correction pressure is small. To this purpose a pressure update formula is used in which after every time step the pressure is updated with a fraction of the correction pressure. It is shown that for stability this fraction may not exceed one. The way in which the pressure is updated may affect the global accuracy of the pressure. The value of the fraction may be tuned or another pressure update formula may be used to optimize the accuracy, but this has not been investigated in further detail.

Finally, Pourquie and Nieuwstadt[7] have shown that the extension of the present IBM to the transport equation for a scalar is straightforward and accurate as well. Both Neumann and Dirichlet boundary conditions can be dealt with by adding an extra term to the scalar transport equation similar to the additional force term in the momentum equation.

REFERENCES

[1] R. Mittal and G. Iaccarino. Immersed boundary methods. *Annual Review of Fluid Mechanics*, **37**, 239–261, (2005).

[2] S. Leonardi, P. Orlandi, R.J. Smalley, L. Djenidi and R.A. Antonia. Direct numerical simulations of turbulent channel flow with transverse square bars on one wall. *Journal of Fluid Mechanics*, **491**, 229–238, (2003).

[3] E.A. Fadlun, R. Verzicco, P. Orlandi and J. Mohd-Yusof. Combined immersed–boundary finite–difference methods for three–dimensional complex flow simulations. *Journal of Computational Physics*, **161**, 35–60, (2000).

[4] W.P. Breugem, B.J. Boersma and R.E. Uittenbogaard. Direct Numerical Simulations of plane channel flow over a 3D Cartesian grid of cubes. In A.H. Reis and

A.F. Miguel, editors, *Applications of Porous Media*, 27–35. Evora Geophysics Center, Evora, (2004).

[5] W.P. Breugem and B.J. Boersma. Direct Numerical Simulations of turbulent flow over a permeable wall using a direct and a continuum approach. *Physics of Fluids*, **17(2)**, (2005).

[6] P. Wesseling. *Principles of computational fluid dynamics*, Springer, (2001).

[7] M. Pourquie and F. Nieuwstadt. The use of virtual boundary conditions for fast DNS/LES of flow around objects. *Proceedings of the 2005 joint ASME/ASCE/SES conference on mechanics and materials (McMAT2005).* Baton Rouge (Louisiana, USA), paper 523, (2005).